CHAPTER 5

Compact Ultra-wideband Filtering Antenna with High Selectivity and Improved Performance

5.1 Introduction

In February 2002, the U.S. Federal Communications Commission (FCC) authorized the unlicensed use of UWB technology for imaging, vehicular radar, indoor high data rate communications [FCC (2002), Aiello and Rogerson (2003), Yang and Giannakis (2004), Adamiuk *et al*. (2012)]. Research effort in the academic and industrial spheres has recently been intensified in the design and development of UWB antennas [Amini *et al*. (2015), Pandey and Meshram (2015), Liang *et al*. (2005), Li *et al*. (2006), Azenui and Yang (2007), Ahmed and Sebak (2008), Sayidmarie and Fadhel (2012), Lin *et al*. (2012), Abed *et al*. (2013), Tripathi *et al*. (2014), Tang *et al*. (2016), Hossain *et al*. (2016), Sam and Zakaria (2017), Ranjan *et al*. (2017)] covering whole UWB frequency band in the range 3.1 – 10.6 GHz. Among various types of UWB antennas, the planar UWB monopole antennas (MPAs) of various shapes viz rectangular, circular, and elliptical shapes [Liang *et al*. (2005), Li *et al*. (2006), Azenui and Yang (2007), Ahmed and Sebak (2008), Sayidmarie and Fadhel (2012), Lin *et al*. (2012), Abed *et al*. (2013), Tripathi *et al*. (2014), Tang *et al*. (2016), Hossain *et al*. (2016), Sam and Zakaria (2017), Ranjan *et al*. (2017)] have been of particular research interest because of their compact size, simple structure, wide frequency impedance bandwidth, easy fabrication and omnidirectional radiation patterns. The UWB monopole antennas using circular-shaped patch is reported in [Liang *et al*. (2005), Li *et al*. (2006), Sam and Zakaria (2017)] while elliptical-shaped patch has been used to obtain UWB MPA in [Li *et al*.

(2006), Azenui and Yang (2007), Sayidmarie and Fadhel (2012), Tang *et al*. (2016)]. The UWB antennas using the flower-shaped patch, and hexagonal-shaped patch with Koch fractal geometry are respectively reported in [Ranjan *et al*. (2017)] and [Tripathi *et al*. (2014)]. In [Ahmed and Sebak (2008)], UWB antenna consisting of stepped-rectangular patch and half circular disc with the circular slot is reported while UWB antenna using the ring-shaped patch with slot and upper cutting edge is reported in [Hossain *et al*. (2016)]. In [Abed *et al*. (2013)], UWB slot antenna is reported using the stepped-circular-shaped slot and stepped-circular stub. The reported UWB antennas are large in size and hence need was felt to miniaturize these antennas. Also, these UWB antennas have some other drawbacks, such as poor band-edge selectivity and presence of unwanted harmonics. Due to these drawbacks, chances of unwanted frequency components being received by the antennas can not be ruled out. This would affect the performance of systems using these antennas. Hence, the antenna is usually followed by a suitable bandpass filter (BPF) to improve its performance over the frequency band of operation and to suppress unwanted harmonics.

To improve the signal-to-noise ratio (S/N) performance of the receiver, it is imperative to keep low noise amplifier (LNA), which includes BPF in its circuit, in close proximity with the antenna by reducing the length of transmission line connecting the antenna to LNA. Therefore, need was felt by researchers to integrate filter and antenna into a single component, known as filtering antenna that performs filtering and radiation functions simultaneously. Various types of filtering antennas are available in the literature [Abbaspour-Tamijani *et al*. (2002), Zuo *et al*. (2009), Chen and Zhou (2009), Mandal and Chen (2010), Wu *et al*. (2011), Djaiz *et al*. (2011), Wu *et al*. (2013), Wong *et al*. (2013), Mansour *et al*. (2014), Sun *et al*. (2016), Tang *et al*. (2016), Ranjan *et al*. (2017), Feng *et al*. (2017), Sahoo *et al*. (2017)]. Out of various types of

filtering antennas, the UWB filtering antennas have been of particular research interest in order to fulfil the requirements of UWB systems. Hence, to design a UWB filtering antenna, efforts have been made to integrate a UWB BPF with a UWB antenna. In [Tang *et al*. (2016), Ranjan *et al*. (2017), Chen and Zhou (2009), Djaiz *et al*. (2011), Sahoo *et al*. (2017)], UWB BPF and UWB antenna are integrated to obtain UWB filter-antenna system. The reported UWB filtering antennas need improvement in terms of size and out-of-band performance. In [Wong *et al*. (2013)], UWB filtering antenna is reported with shorting pins to improve the in-band selectivity. Although the reported UWB filter antenna is compact and has good in-band selectivity but it requires improvement in terms of out-of-band performance.

In this chapter, a new compact UWB filtering antenna having good cut-off performance and wide stopband with highly suppressed unwanted harmonics is presented. The UWB filtering antenna is obtained through integration of modified elliptic-shaped UWB antenna with optimized version of compact UWB BPF described in **chapter 4**. The UWB BPF is responsible for obtaining improved cut-off performance with suppression of unwanted harmonics. Initially, a compact modified elliptic-shaped UWB antenna is designed and analysed through numerical simulation and experimental studies. Further, a compact UWB BPF presented in chapter 4 is optimized to obtain desired reflection and transmission characteristics using numerical simulation software. The optimized UWB BPF is integrated with the proposed UWB antenna without any extra matching circuit to achieve compact integrated system with good impedance matching within the desired passband. The proposed integrated system is called the UWB filtering antenna. The proposed UWB filtering antenna is analysed through numerical simulation and experimental studies. The numerical simulation study of UWB antenna and UWB filtering antenna is carried out using Ansys high-frequency

structure simulator (HFSS) numerical simulation software. Roger RT/duroid 5880 substrate (ε_r = 2.2, tanδ = 0.0006, thickness = 0.787mm) was used for design, simulation and experimental studies of the proposed UWB antenna and the proposed UWB filtering antenna. The time domain analyses of the proposed UWB antenna and UWB filtering antenna are also carried out using finite integration technique (FIT) based Computer Simulation Technology Microwave Studio (CST MWS) software.

5.2 Proposed Compact UWB Monopole Antenna

5.2.1 Design and Investigation of the Proposed UWB Antenna

The geometrical configuration of the proposed UWB MPA along with its shape parameters is shown in Figure 5.2(a). The proposed UWB MPA is evolved from a simple circular-shaped UWB MPA. The design stages involved in the evolution of the proposed UWB antenna from a conventional circular-shaped MPA is shown in Figure 5.1. Figure 5.1 shows the geometries of four shapes of UWB MPAs along with the proposed UWB antenna. Circular-shaped MPA with the partial rectangular ground plane and modified ground plane have been designated as 'Type-I' and 'Type-II' antennas respectively, whereas elliptic-shaped MPA with modified ground plane has been designated as 'Type-III' antenna. 'Type-IV' antenna consists of a combination of two modified elliptic-shaped patches with modified ground plane. Roger RT/duroid 5880 substrate material (ε_r = 2.2, tanδ = 0.0009 and thickness = 0.787 mm) was used for design of all MPAs along with the proposed UWB antenna. The proposed UWB antenna consists of a combination of three modified elliptic-shaped patches and modified ground plane fed through a 50 Ω microstrip line with tapered transition. The top side of the proposed antenna consists of a combination of three modified elliptic-shaped patches connected to 50 Ω microstrip feedline through a tapered transition. The

combination of modified elliptic-shaped patches is responsible for increasing the electrical length of the proposed UWB antenna and hence, its resonant frequency shifts to lower side without increase in its physical size which makes the proposed antenna more compact. The bottom side of the proposed antenna contains modified ground plane having curved shape and a rectangular cut in the central region of its upper side. The combination of modified elliptic-shaped patches and modified ground plane are responsible for good impedance matching over the desired UWB frequency range 3.1 – 10.6 GHz. The rectangular slot efficiently tunes the mutual coupling between the radiating element and the ground over a wide frequency range. The curved shape in the upper region of the ground plane is introduced for smooth transition from one resonant mode to another across the UWB frequency range [Lin *et al*. (2012)] and it ensures good impedance matching over the entire UWB frequency range. The values of optimized geometrical parameters of the proposed UWB antenna are given in Table 5.1. The overall size of the proposed UWB antenna is 37 mm × 21 mm × 0.787 mm. The basic shapes of UWB MPA along with the proposed UWB antenna have been designed and numerically simulated in order to compare their reflection coefficient-frequency characteristics. For a fair comparison, physical size of all the antennas including the proposed UWB antenna was kept same.

In order to understand the operating mechanisms of various types of MPA structures along with the proposed one, the current distributions on the surfaces of these antenna configurations are discussed. Figure 5.3 depicts the surface current distributions for various types of MPA configurations at the frequencies of 3.1, 6.8, and 10.6 GHz. From Figure 5.3, it can be observed that more or equivalent current is concentrated on the surface of the proposed UWB antenna as compared to other antenna configurations at different frequencies of interest. Hence, it can be said that the proposed antenna

configuration is properly excited to provide better performance as compared to other investigated antenna configurations.

Figure 5.4 shows the simulated variations of reflection coefficient with frequency for five different geometries of antennas, which include 'Type-I', 'Type-II', 'Type-III', 'Type-IV', and the proposed antennas. The objective of present investigation is to design and develop a compact antenna which covers whole UWB frequency range (3.1 – 10.6 GHz) with good impedance matching. To achieve that objective, initially conventional circular-shaped antenna is chosen and ultimately obtained the proposed compact UWB antenna configuration through step-by-step modification in the geometry which provided good impedance matching over whole UWB frequency range. With antenna of Type I/II/III/IV, difficulty is faced in obtaining good impedance matching over whole UWB frequency range (3.1 – 10.6 GHz) without compromising the compactness of the antenna structure. That is why, further modification is done in the geometry and finally devised the proposed compact UWB antenna configuration, which provides good impedance matching over whole UWB frequency range (3.1 – 10.6 GHz). Table 5.2 shows the comparative study in terms of impedance bandwidth for the same physical area of various types of monopole antennas shown in Figure 5.1. From Figure 5.4 and Table 5.2, it can be easily observed that the proposed compact UWB antenna provides widest -10 dB reflection coefficient bandwidth along with good impedance matching over the frequency band of interest (3.1 – 10.6 GHz).

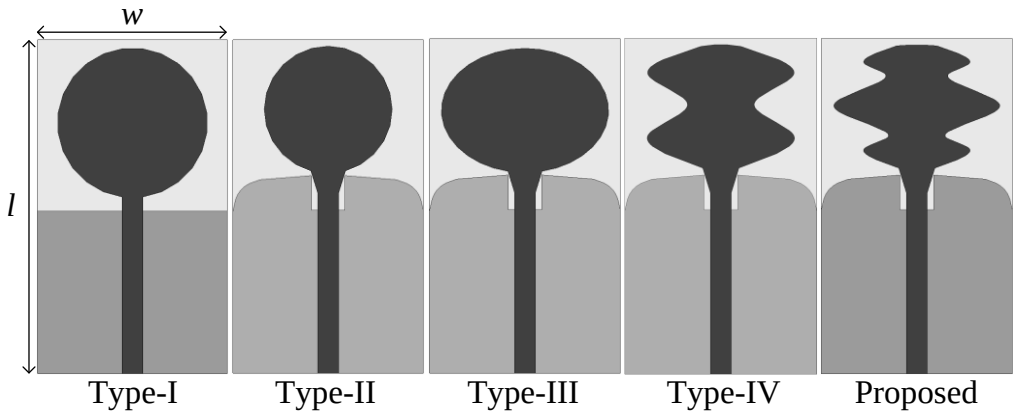

Figure 5.1: Geometries of different monopole antennas: circular-shaped with partial rectangular ground plane (Type-I), circular-shaped with modified ground plane (Type-II), elliptic-shaped with modified ground plane (Type-III), two modified elliptic-shaped with modified ground plane (Type-IV), and three modified elliptic-shaped with modified ground plane (the proposed UWB antenna).

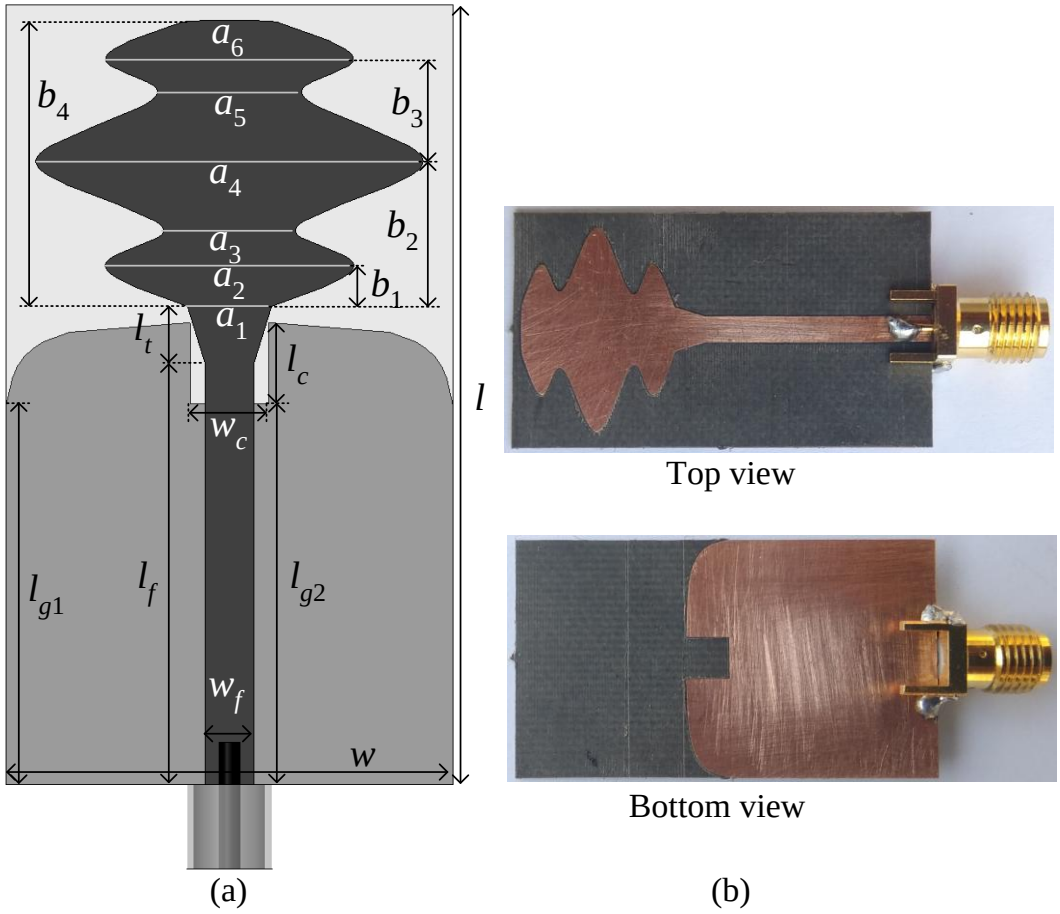

Figure 5.2: (a) Geometry of the proposed modified elliptic-shaped UWB antenna. (b) Top and bottom views of the fabricated prototype of the proposed UWB antenna.

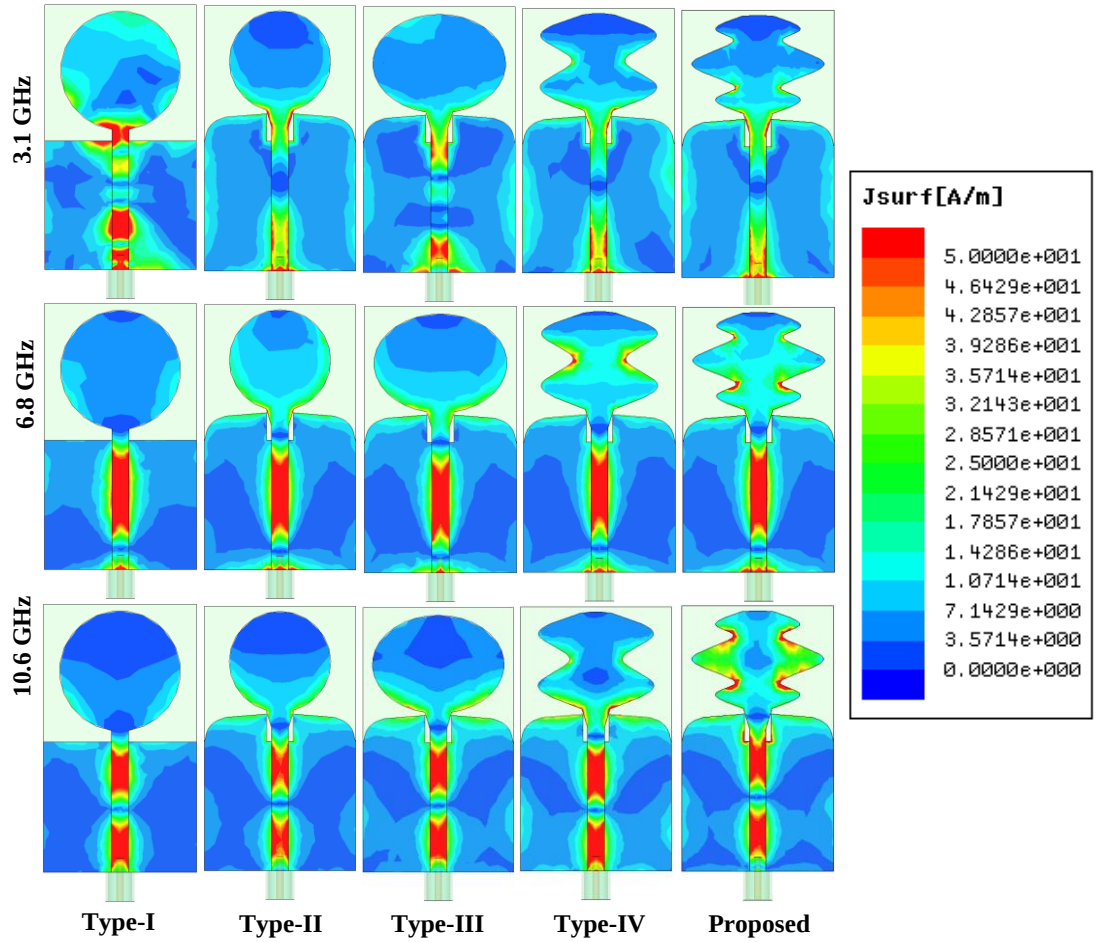

Figure 5.3: Simulated surface current distribution for different geometries (Type-I, Type-II, Type-III, Type-IV, and Proposed) of the monopole antennas at different frequencies of 3.1, 6.8, and 10.6 GHz.

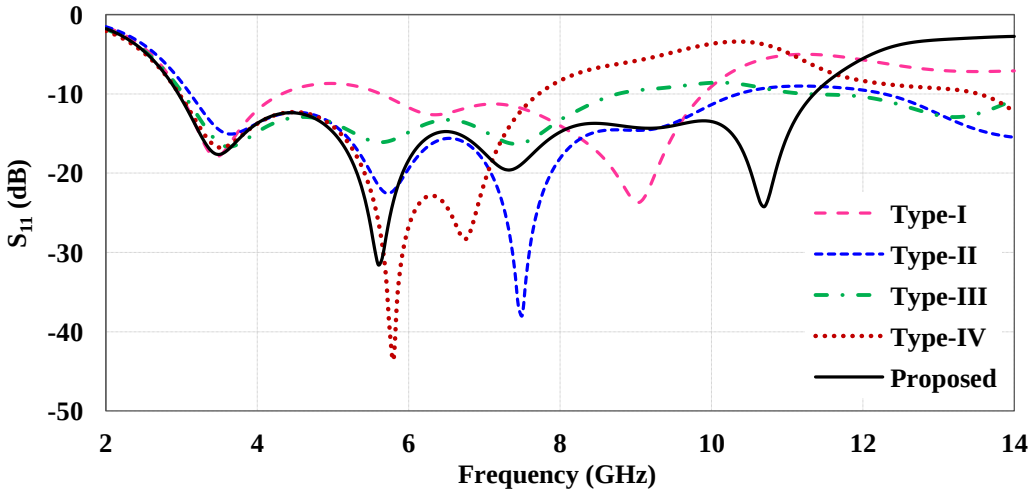

Figure 5.4: Numerically simulated variations of reflection coefficient with frequency for different geometries (Type-I, Type-II, Type-III, Type-IV, and Proposed) of the monopole antennas.

Further, the proposed UWB antenna is numerically simulated for its radiation patterns, realized gain-frequency characteristic, total efficiency-frequency characteristic and pulse handling capability in addition to its input characteristic. Furthermore, the prototype of the proposed UWB antenna was fabricated using printed circuit board (PCB) Technology for experimental study in order to validate the simulation results for antenna's input characteristic, radiation patterns and realized gain-frequency characteristic. Figure 5.2(b) shows the top and bottom views of the fabricated prototype of the proposed modified elliptic-shaped UWB antenna. A sub-miniature version A (SMA) connector was used for feeding the RF power to the antenna through microstrip line as shown in Figure 5.2(b).

Table 5.1: Optimized geometrical parameter values of the proposed modified elliptic-shaped UWB antenna (all dimensions are in millimeter).

l = 37	w = 21	w_f = 2.3	l_{g1} = 18	l_f = 20
l_t = 2.7	l_{g2} = 18.1	l_c = 3.83	w_c = 3.7	a_1 = 3.95
a_2 = 11.67	a_3 = 6.2	a_4 = 18.2	a_5 = 6.77	a_6 = 11.65
b_1 = 1.96	b_2 = 6.89	b_3 = 4.85	b_4 = 13.6	–

Table 5.2: Comparison of various types of monopole antennas in terms of bandwidth and physical area.

Types of monopole antennas	Impedance Bandwidth
Type-I	(1.34 GHz) 2.88 – 4.22 GHz & (4.27 GHz) 5.52 – 9.79 GHz
Type-II	(7.24 GHz) 3.12 – 10.36 GHz
Type-III	(5.75 GHz) 3.02 – 8.77 GHz
Type-IV	(4.75 GHz) 2.97 – 7.72 GHz
Proposed	(8.4 GHz) 2.96 – 11.36 GHz

*The physical area for all types of monopole antennas is same (= 37 mm × 21 mm).

5.2.2 Results and Discussion

5.2.2.1 Reflection Coefficient-Frequency Characteristics

Figure 5.5 shows numerically simulated and measured variations of reflection coefficient of the proposed UWB antenna with frequency. From Figure 5.5, it can be observed that simulated -10 dB reflection coefficient bandwidth of the proposed UWB antenna covers the frequency range 2.96 – 11.36 GHz. It can also be observed that at and around simulated frequency of 18.5 GHz, unwanted harmonics are present. Because of the presence of unwanted harmonics, signal interference occurs in the wireless system and it affects the S/N performance of the receiver circuitry. Hence, in order to achieve better S/N performance of receiver circuitry in a wireless system, out-of-band harmonics should be suppressed. Although the simulation study of the antenna was carried out up to 30 GHz, measurement was made up to 18 GHz due to the limited operating frequency range of respective equipments/components available in our laboratory. The magnitudes of reflection coefficient of the proposed UWB antenna were measured over the frequency range 2–18 GHz using Anritsu make vector network analyser (VNA) Master (Model: MS2038C). The measured -10 dB reflection coefficient bandwidth of the proposed UWB antenna covers the frequency range 3.01 – 11.2 GHz. It can be seen from Figure 5.5 that the simulated and measured results are nearly in agreement with each other over the frequency range of interest. The deviation in simulation and measured results is due to fabrication tolerances and measurement errors.

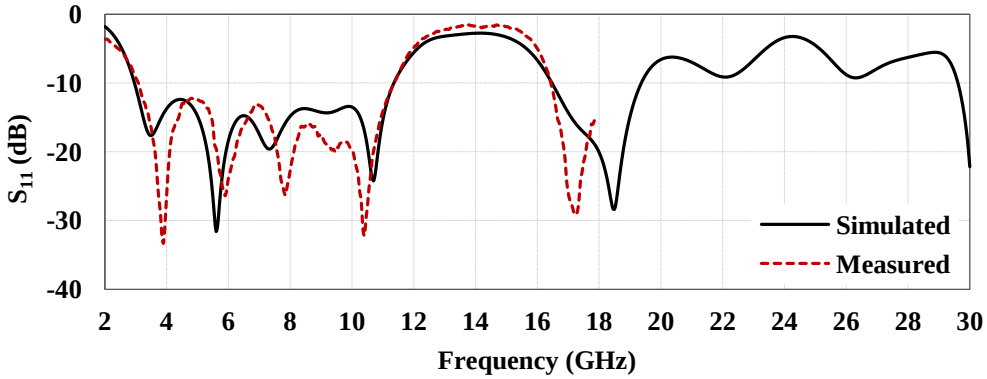

Figure 5.5: Numerically simulated and measured variations of reflection coefficient of the proposed UWB antenna with frequency.

5.2.2.2 Radiation Patterns and Peak Realized Gain-Frequency Characteristics

The simulated and measured co- and cross-polarized radiation pattern plots of the proposed UWB antenna in E- and H-planes for four different frequencies (3.5, 5.5, 7.5, 9.5 GHz) which are within operating frequency band are presented in Figure 5.6. From Figure 5.6, it can be observed that the proposed UWB antenna exhibits omni-directional co-polar radiation patterns with low cross-polarization levels at the frequencies of interest.

Figure 5.7 shows the simulated and measured variations of realized gain values of the proposed UWB antenna with frequency. Although the simulation study of the antenna was carried out up to 30 GHz, measurement was made up to 18 GHz due to the limited operating frequency range of respective equipments/components available in our laboratory. The simulated (measured) realized gain values vary in the range 2.26 – 5.2 dB (2.25 – 4.64 dB) over the operating frequency range 2.96 – 11.36 GHz (3.01 – 11.2 GHz). In the undesired frequency range, the simulated realized gain values initially decreases but starts increasing from 14.1 GHz and peaks at 17.2 GHz, where its value reaches 4.96 dB. Thereafter, it shows decreasing trend upto 24.5 GHz and finally more or less increasing trend in the frequency range 24.5 – 30 GHz.

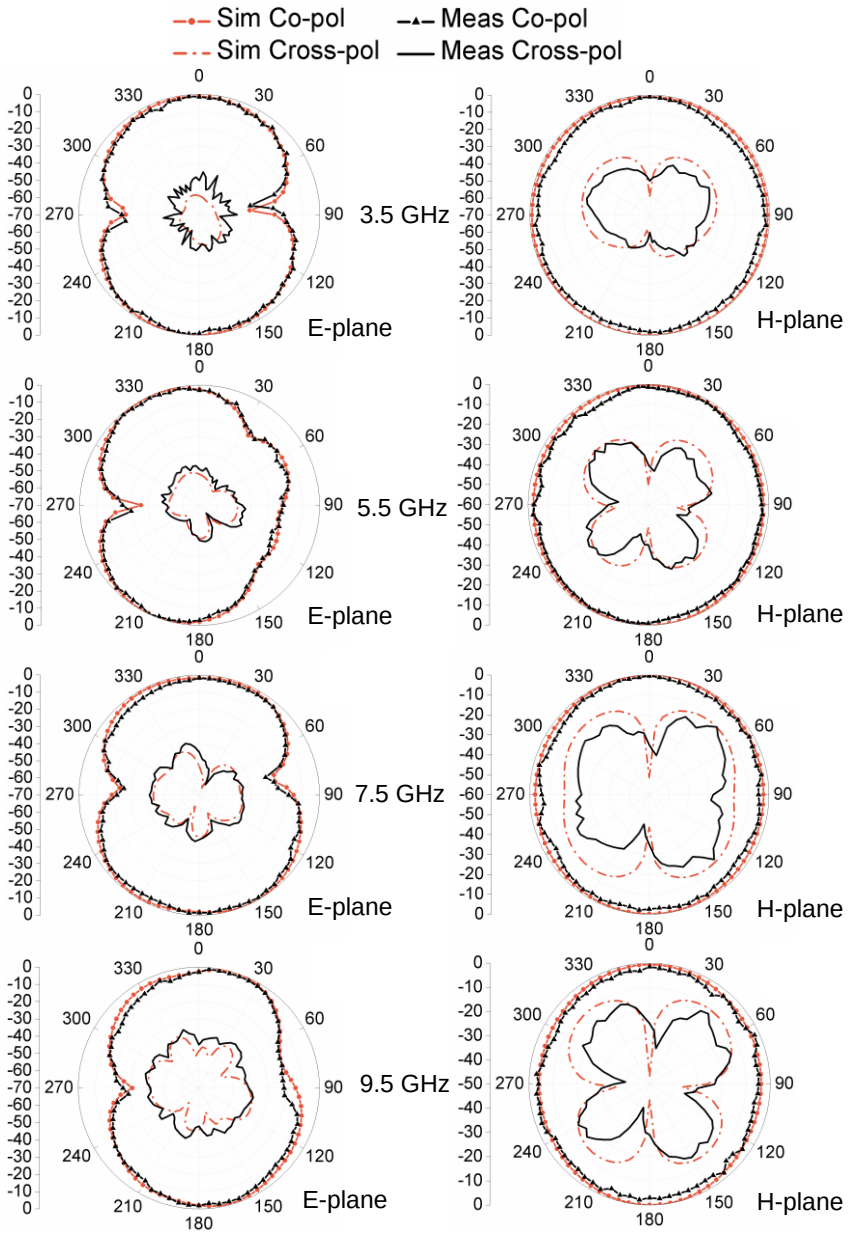

Figure 5.6: Numerically simulated and measured radiation patterns of the proposed UWB antenna for four different frequencies 3.5, 5.5, 7.5, 9.5 GHz.

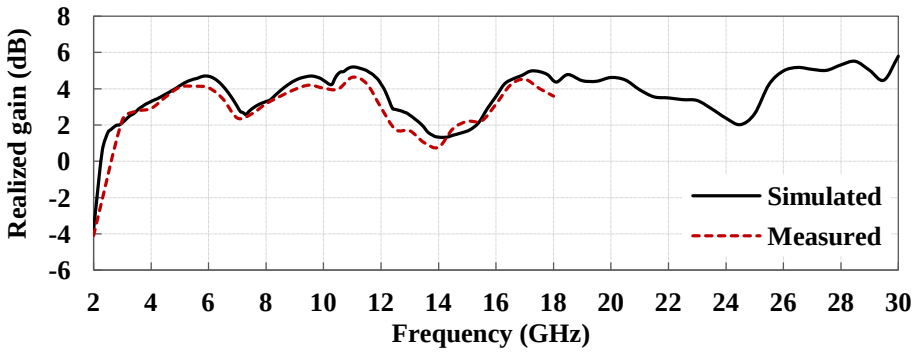

Figure 5.7: Numerically simulated and measured gain values of the proposed UWB antenna as functions of frequency.

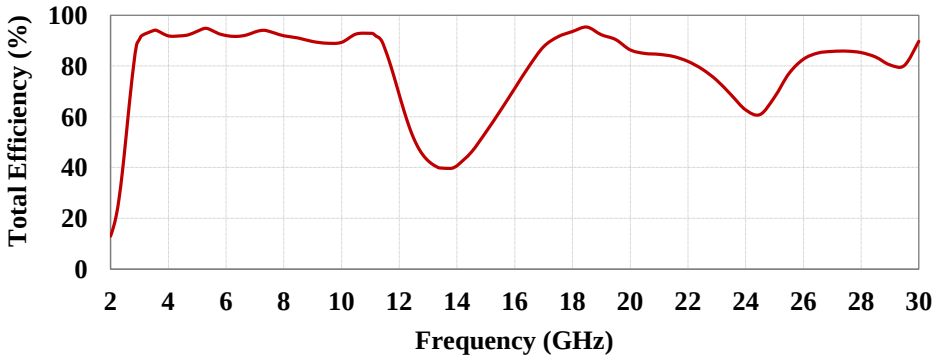

Figure 5.8: Simulated total efficiency of the proposed UWB antenna as a function of frequency.

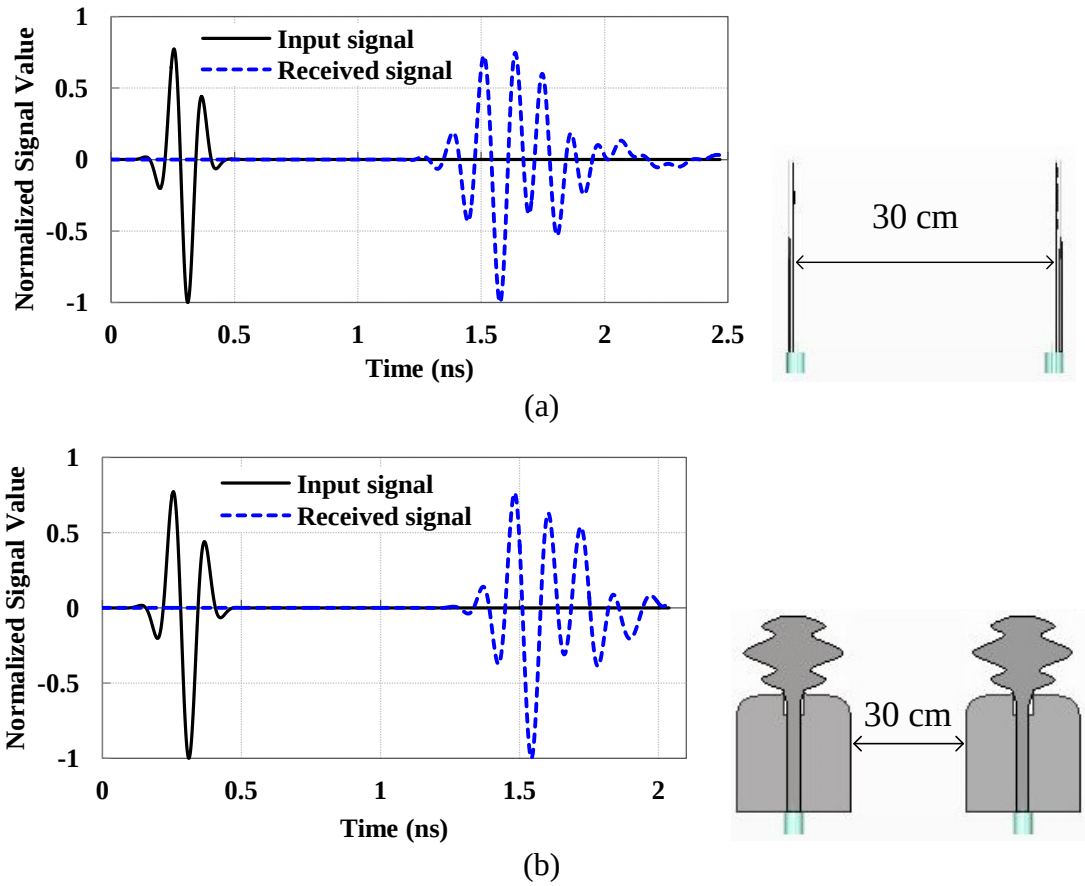

Figure 5.9: Excited and received pulses for different orientations of proposed UWB antennas at a distance of 30 cm (a) face-to-face, and (b) side-by-side.

5.2.2.3 Simulated Total Efficiency-Frequency Characteristic

Figure 5.8 shows the simulated variation of total efficiency of the proposed UWB antenna with frequency. From the Figure 5.8, it can be observed that values of total efficiency vary over the range 89 – 94 % in the desired UWB passband 2.96 – 11.36

GHz. In the undesired upper frequency range, the total efficiency initially decreases but starts increasing from 13.8 GHz and peaks at 18.5 GHz, where its value reaches ~ 95 %. Thereafter, it shows decreasing trend upto 24.5 GHz, where its value is 60.9 % and then it increases to 85.8 % at 27.5 GHz starting from 60.9 % at 24.5 GHz. The total efficiency of the antenna shows decreasing trend again in the frequency range 27.5 – 29.5 GHz, where its value changes from 85.8 % to 80.2 %. Finally, total efficiency shows increasing trend in the frequency range 29.5 – 30 GHz, where its value increases from 80.2 % to 89.7 %.

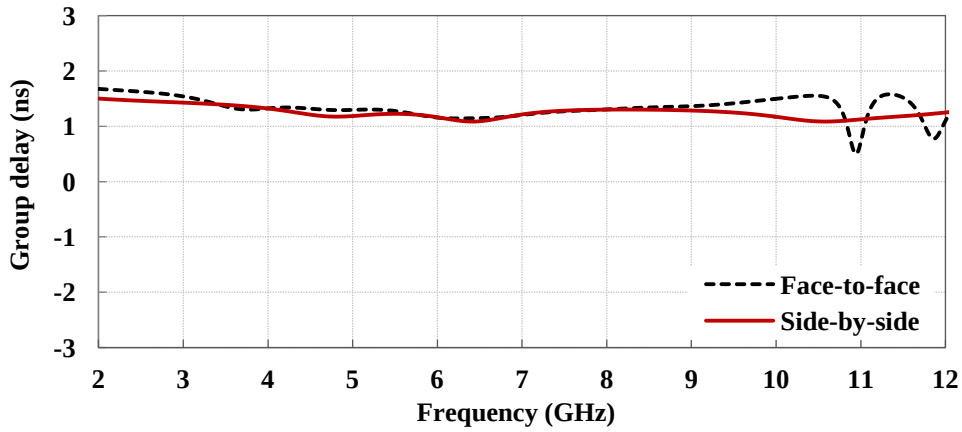

Figure 5.10: Simulated far-field group delays of proposed UWB antenna for different orientations at a distance of 30 cm.

5.2.2.4 Time Domain Analysis

One of the important performance indicators of UWB antennas is their pulse handling capability. It can be studied through time domain analysis and fidelity factor calculation in the far-field region in face-to-face and side-by-side orientations with respect to transmitting antenna using finite integration technique (FIT) based computer simulation technology microwave studio (CST MWS) software. The transmitting antenna was excited with Gaussian pulse and the signal was received at the receiving antenna kept at a distance of 30 cm in the far-field region. The normalized amplitudes of excited and

received signals are shown in Figure 5.9. This figure depicts that the received pulse is similar to that transmitted which indicates that distortion in received signal is insignificant. The correlation between excited and received signals is calculated using the expression for system fidelity factor (SFF) [Quintero et al. (2011)] given as

$$\hat{R}_s(t) = \frac{R_s(t)}{\left[\int_{-\infty}^{\infty} |R_s(t)^2| dt\right]^2} \tag{5.1}$$

$$\hat{T}_s(t) = \frac{T_s(t)}{\left[\int_{-\infty}^{\infty} |T_s(t)^2| dt\right]^2} \tag{5.2}$$

$$SFF = max \int_{-\infty}^{\infty} \hat{T}_s(t)\, \hat{R}_s(t+\tau) dt \tag{5.3}$$

where, $\hat{R}_s(t)$ and $\hat{T}_s(t)$ are the normalized received and transmitted signals. The system fidelity factors (SFFs) in the case of face-to-face and side-by-side orientations are found to be 0.81 and 0.87 respectively. The calculated SFF values are close to unity showing that the antenna has good pulse handling characteristics.

Another important parameter of UWB antennas is their almost constant group delay over the whole operating frequency band. The group delay is used to represent the degree of pulse signal distortion. The simulated values of far-field group delay was obtained using arrangements of transmitting and receiving antennas identical to those employed for time domain analysis explained earlier. The variations of far-field group delay of the proposed antenna for face-to-face and side-by-side configurations with frequency were determined through simulation using CST MWS software and the results are provided in Figure 5.10. It can be seen from Figure 5.10 that the simulated values of far-field group delay of the proposed antenna vary in the range 0.5−1.55 ns for face-to-face and side-by-side configurations over the whole operating frequency band.

5.2.2.5 Performance Comparison of the Proposed UWB Antenna with Those Reported in Literature

Further, the dimension and performance based comparison of the proposed UWB antenna with those reported in the literature is given in Table 5.3. It is apparent from Table 5.3 that the proposed UWB antenna is more compact and covers the whole UWB band. The proposed UWB antenna provides almost stable radiation patterns with reasonably good realized gain values over the UWB frequency band. However, the proposed UWB antenna needs improvement in terms of cut-off performance in UWB frequency band and suppression of out-of-band (unwanted) harmonics.

Table 5.3: Comparison of the proposed UWB antenna with the UWB antennas reported in the literature.

Reference	-10 dB reflection coefficient bandwidth (GHz)	Size (mm × mm)	Substrate dielectric constant, and height (mm)
[Liang *et al*. (2005)]	2.69 – 10.16	42 × 50	4.7, 1.5
[Azenui and Yang (2007)]	2.7 – 12.0	45 × 50	4.2, 0.762
[Ahmed and Sebak (2008)]	3 – 11.4	50 × 41	2.2, 1.575
[Sayidmarie and Fadhel (2012)]	2.83 – 13.7	46 × 44	4.3, 1.6
[Abed *et al*. (2013)]	2.21 – 11.5	42 × 48	4.32, 1.59
[Tripathi *et al*. (2014)]	3.0 – 12.8	31 × 28	4.4, 1.6
[Tang *et al*. (2016)]	2.615 – 14.0	37 × 25	3.48, 1.524
[Hossain *et al*. (2016)]	3.088 – 12.497	35 × 24	4.4, 1.6
[Sam and Zakaria (2017)]	3.048 – 10.561	40 × 29	3.48, 0.508
[Ranjan *et al*. (2017)]	3.1 – 14.0	30 × 25	3.38, 1.524
Proposed antenna	**2.96 – 11.36**	**37 × 21**	**2.2, 0.787**

5.3 Ultra-wideband (UWB) Bandpass Filter (BPF)

5.3.1 Design of UWB BPF

In order to improve in-band cut-off performance and suppression of unwanted harmonics of the proposed UWB antenna, the compact UWB BPF presented in **chapter 4** is used. Figure 5.11 shows the geometry of the compact UWB BPF having sharp cut-off performance and wide stopband with high rejection capability. Figure 5.11(a) and (b) show the top and bottom views of the UWB BPF. The UWB BPF shown in Figure 5.11(c) is obtained through integration of modified multimode resonator (MMR)-based UWB BPF (shown in Figure 5.11(a)) and defected ground structure (DGS)-based lowpass filter (LPF) (shown in Figure 5.11(b)) . The detailed procedure for design of compact UWB BPF is available in chapter 4. For accommodating the operational UWB frequency band of the proposed modified elliptic-shaped antenna, the design parameters of the compact UWB BPF have been optimized in order to realize the desired reflection and transmission performance characteristics. It is to be noted that certain design principles were considered during optimization of the BPF's parameters for its integration with the proposed UWB antenna. First, the dielectric substrate employed for the BPF should be same as that used for the antenna. Second, the characteristic impedance of the microstrip line feeds at the input and output ports of the filter must be equal to 50 Ω i.e. the microstrip line width at the input and output ports of the filter should be same as the width of line at the antenna input and both should meet 50 Ω impedance criterion. Third, the -10 dB reflection coefficient bandwidth of the filter should cover atleast UWB frequency range i.e. 3.1 – 10.6 GHz. The dielectric substrate, RT/duroid 5880 having thickness of 0.787 mm was chosen for the design of the BPF. Further, the geometrical parameters of the BPF have been optimized using numerical simulation software for obtaining desired reflection coefficient bandwidth. The

optimized values of the geometrical parameters of the BPF are given in Table 5.4. The overall size of the compact UWB BPF having optimized parameters is 14.03 mm × 5.83 mm × 0.787 mm.

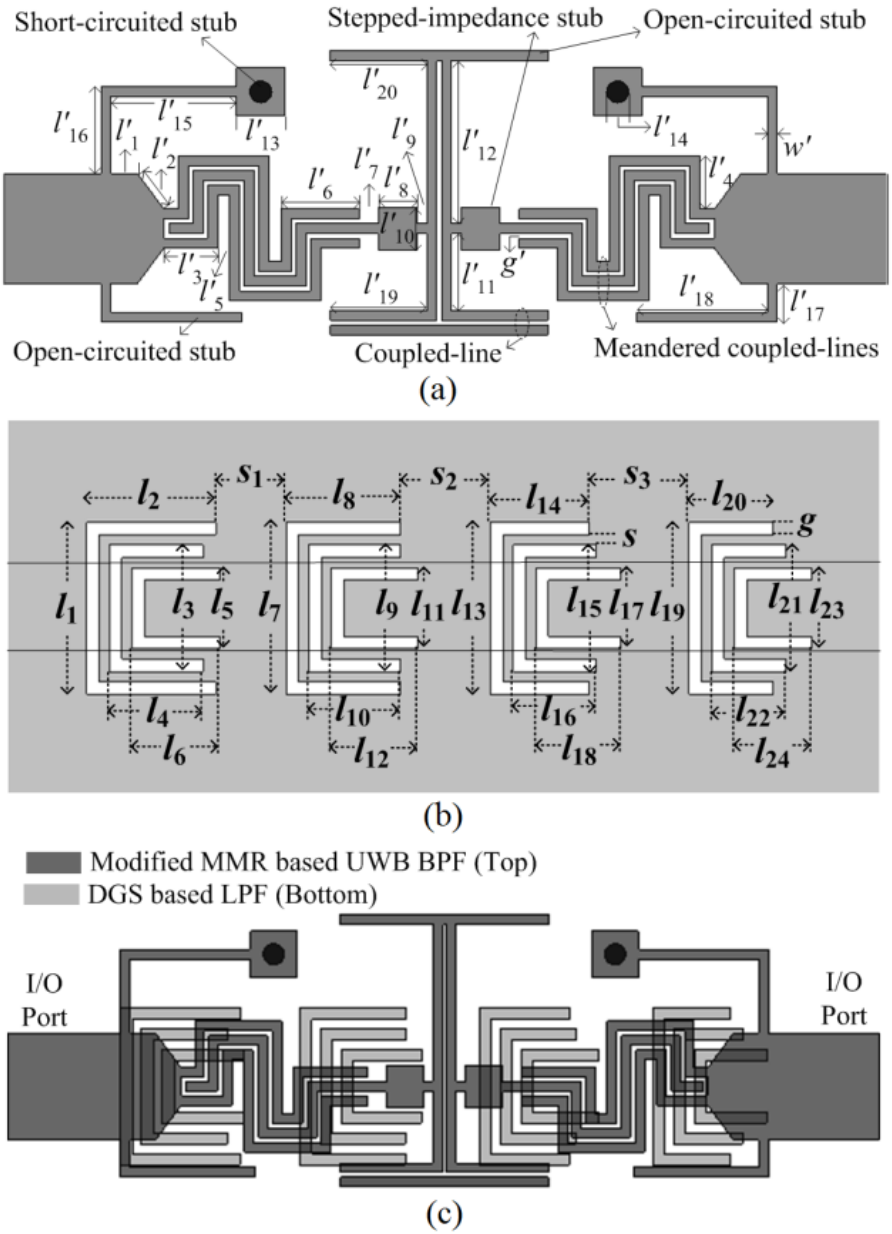

Figure 5.11: The geometry of the UWB BPF integrated with DGS-based LPF (a) Top view, (b) Bottom view, and (c) Proposed compact UWB BPF.

5.3.2 Results and Discussion

The simulated variations of S-parameters of the optimized compact UWB BPF with frequency are shown in Figure 5.12. From Figure 5.12, it can be observed that -10 dB

reflection coefficient bandwidth of the BPF is 7.75 GHz (= 111.9 %) and covers the frequency range 3.05–10.8 GHz. The 3-dB passband frequency range of the BPF is 2.81 – 10.85 GHz. As far as stopband performance is concerned, upper stopband attenuation level is better than 39.3 dB up to 20.7 GHz and 21.8 dB up to 30 GHz. The maximum value of simulated insertion loss at a mid-band frequency of the filter passband is found to be 0.52 dB.

Table 5.4: Optimized geometrical parameter values of the compact UWB BPF (all dimensions are in millimeter)

$l'_1 = 0.57$	$l'_2 = 0.94$	$l'_3 = 1.12$	$l'_4 = 0.99$	$l'_5 = 0.25$	$l'_6 = 1.63$
$l'_7 = 0.35$	$l'_8 = 0.81$	$l'_9 = 0.2032$	$l'_{10} = 0.91$	$l'_{11} = 1.53$	$l'_{12} = 3.39$
$l'_{13} = 1.0$	$l'_{14} = 0.46$	$l'_{15} = 2.7$	$l'_{16} = 1.8$	$l'_{17} = 0.83$	$l'_{18} = 2.74$
$l'_{19} = 1.99$	$l'_{20} = 2.02$	$g' = 0.1016$	$w' = 0.2032$	$l_1 = 3.4$	$l_2 = 2.57$
$l_3 = 2.49$	$l_4 = 1.87$	$l_5 = 1.61$	$l_6 = 1.74$	$l_7 = 3.42$	$l_8 = 2.28$
$l_9 = 2.49$	$l_{10} = 1.83$	$l_{11} = 1.61$	$l_{12} = 1.72$	$l_{13} = 3.41$	$l_{14} = 1.95$
$l_{15} = 2.51$	$l_{16} = 1.66$	$l_{17} = 1.61$	$l_{18} = 1.71$	$l_{19} = 3.4$	$l_{20} = 1.68$
$l_{21} = 2.51$	$l_{22} = 1.47$	$l_{23} = 1.61$	$l_{24} = 1.54$	$S = 0.2$	$g = 0.25$
$S_1 = 1.28$	$S_2 = 1.60$	$S_3 = 1.77$	–	–	–

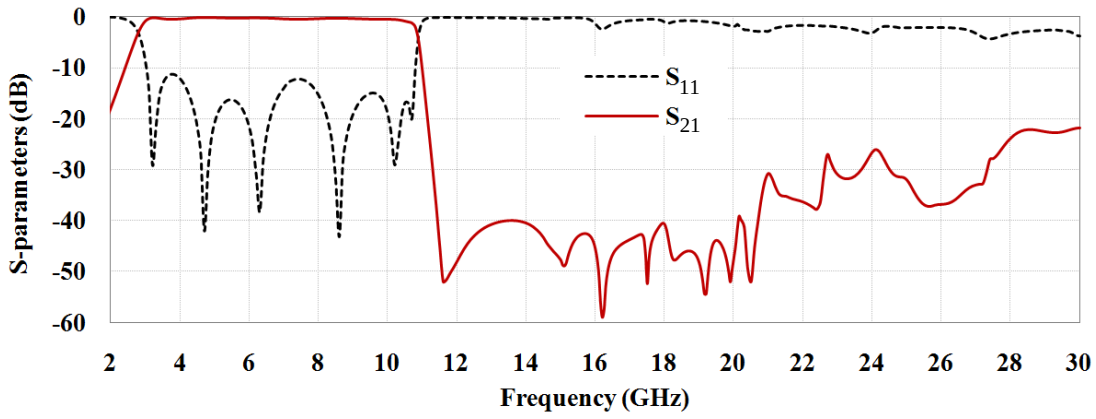

Figure 5.12: Numerically simulated variations of S-parameters of the compact UWB BPF versus frequency.

5.4 Proposed UWB Filtering Antenna

5.4.1 Design and Investigation of the UWB Filtering Antenna

The modified elliptic-shaped UWB antenna was integrated with the optimized compact UWB BPF and the geometrical parameters of the integrated system were optimized in order to obtain the proposed compact UWB filtering antenna having highly suppressed unwanted harmonics with improved band-edge selectivity. Figure 5.13 shows three different designs of modified elliptic-shaped antenna integrated with BPF. In the first integrated system [shown in Figure 5.13(a)], the BPF output is directly connected to the feedline of the modified elliptic-shaped antenna. In the second system [shown in Figure 5.13(b)], the antenna with modified feedline having sharp corners is integrated with BPF while in the third design of integrated system [the propsoed UWB filtering antenna shown in Figure 5.13(c)], the antenna with modified feedline having curved corners is integrated with BPF. Table 5.5 shows the optimized geometrical parameter values of the proposed UWB filtering antenna shown in Figure 5.13(c). Figure 5.14 shows the simulated variations of reflection coefficient with frequency for different geometries of filtering antennas shown in Figure 5.13 which include 'Design-I', 'Design-II', and the proposed UWB filtering antenna. It can be seen from Figure 5.14 that the impedance matching of the directly integrated filtering antenna shown in Figure 5.13(a) is not good in the desired frequency band. In the directly integrated system, impedance mismatch occurs due to loading effect of BPF on the antenna. Further, to improve the impedance matching of the filtering antenna without using extra matching network and without increasing its size, the feedline of the antenna is modified. The BPF is integrated with modified feedline to improve impedance matching over the desired UWB frequency band. Furthermore, the corners of the modified feedline have been curved [as denoted by a parameter '*C*' in Figure 5.13(c)] in order to further improve the impedance

matching over the frequency band of interest and obtain smooth transition from one resonant frequency to another. The optimized geometrical parameter values of the proposed modified elliptic-shaped UWB antenna integrated with the UWB BPF [shown in Figure 5.13(c)] are given in Table 5.5. The proposed integrated design shown in Figure 5.13(c) provides wide impedance bandwidth along with good impedance matching over entire UWB frequency band.

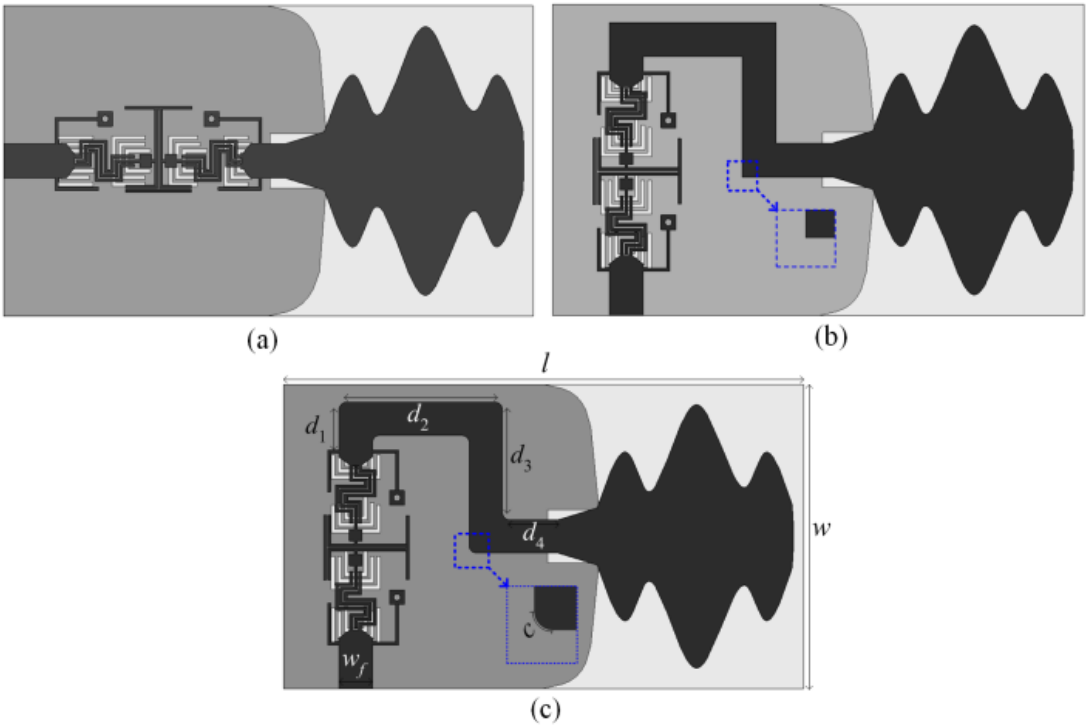

Figure 5.13: The geometries of the modified elliptic-shaped UWB antenna integrated with the compact UWB BPF: (a) Design-I, (b) Design-II, and (c) the proposed filtering antenna.

The prototype of the proposed UWB filtering antenna (shown in Figure 5.13(c)) was fabricated on RT/duroid 5880 substrate (ε_r = 2.2, tanδ = 0.0009, and thickness = 0.787 mm) using PCB technology for experimental study. Figure 5.15 shows top and bottom views of the fabricated prototype of the proposed UWB filtering antenna. The overall size of the proposed compact UWB filtering antenna is 36 mm × 21 mm × 0.787 mm.

The input as well as radiation characteristics along with surface current distributions of the proposed UWB antenna with and without the integration of the UWB BPF are studied through numerical simulation and/or experimentally. Further, the time domain analysis of the proposed UWB filtering antenna is also carried out through CST MWS software to ascertain its pulse handling capability.

Table 5.5: Optimized geometrical parameter values of the proposed UWB Filtering antenna.

l = 36	w = 21	w_f = 2.3	c = 0.8	d_1 = 2.8	d_2 = 10.3
d_3 = 7.12	d_4 = 3.35	l_{g1} = 18	l_t = 2.7	l_{g2} = 18.3	l_c = 3.53
w_c = 3.7	a_1 = 3.95	a_2 = 11.67	a_3 = 6.2	a_4 = 18.2	a_5 = 6.77
a_6 = 11.65	b_1 = 1.96	b_2 = 6.89	b_3 = 4.85	b_4 = 13.6	l'_1 = 0.3
l'_2 = 0.93	l'_3 = 1.11	l'_4 = 1.0	l'_5 = 0.25	l'_6 = 1.61	l'_7 = 0.39
l'_8 = 0.8	l'_9 = 0.2032	l'_{10} = 0.9	l'_{11} = 1.62	l'_{12} = 3.4	l'_{13} = 1.0
l'_{14} = 0.46	l'_{15} = 2.6	l'_{16} = 1.8	l'_{17} = 0.8	l'_{18} = 2.7	l'_{19} = 1.99
l'_{20} = 1.95	g' = 0.1016	w' = 0.2032	l_1 = 3.41	l_2 = 2.58	l_3 = 2.5
l_4 = 1.86	l_5 = 1.61	l_6 = 1.74	l_7 = 3.4	l_8 = 2.28	l_9 = 2.49
l_{10} = 1.84	l_{11} = 1.62	l_{12} = 1.72	l_{13} = 3.42	l_{14} = 1.96	l_{15} = 2.52
l_{16} = 1.66	l_{17} = 1.61	l_{18} = 1.71	l_{19} = 3.40	l_{20} = 1.69	l_{21} = 2.50
l_{22} = 1.48	l_{23} = 1.61	l_{24} = 1.54	S = 0.2	g = 0.25	S_1 = 1.27
S_2 = 1.60	S_3 = 1.77	–	–	–	–

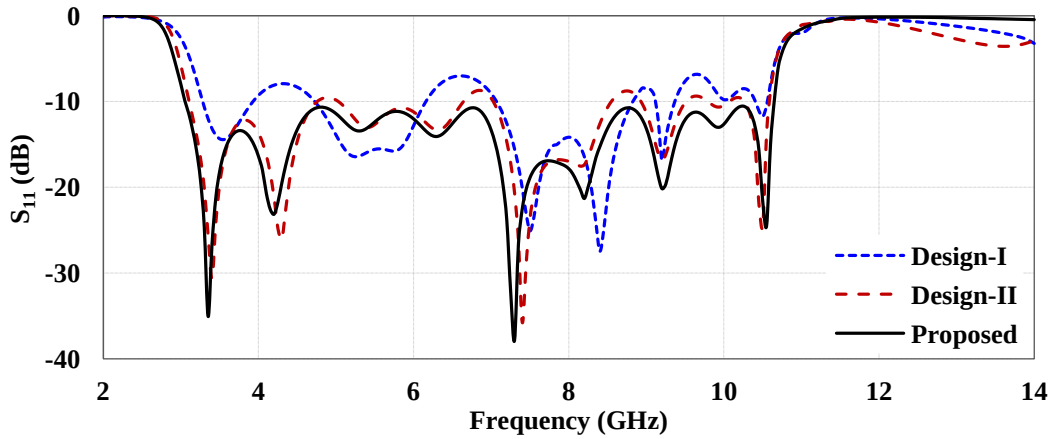

Figure 5.14: Numerically simulated variations of reflection coefficient with frequency for different geometries (Design-I, Design-II, and Proposed) of the modified elliptic-shaped UWB antenna integrated with the compact UWB BPF.

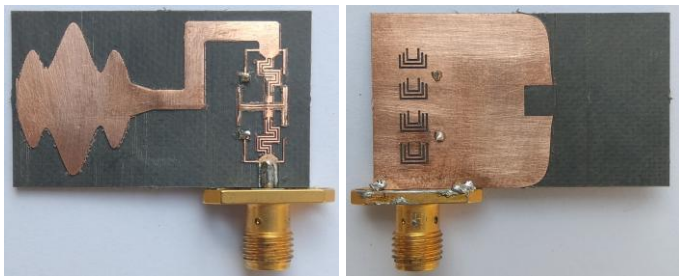

(a) (b)

Figure 5.15: Fabricated prototype of the proposed UWB filtering antenna (a) Top view, and (b) Bottom view.

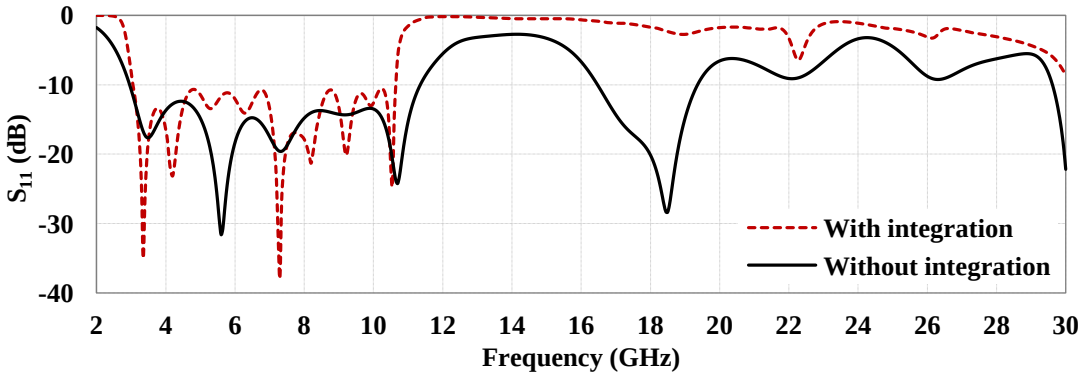

Figure 5.16: Numerically simulated variation of reflection coefficient of the proposed UWB antenna with and without integration of the BPF versus frequency.

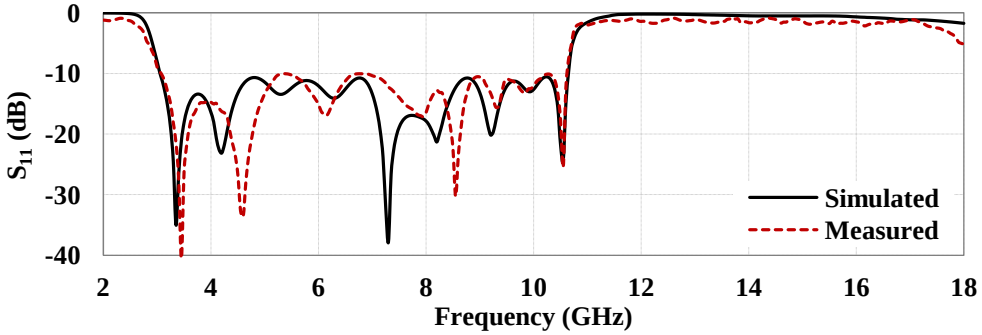

Figure 5.17: Numerically simulated and measured variations of reflection coefficient of the proposed UWB filtering antenna versus frequency.

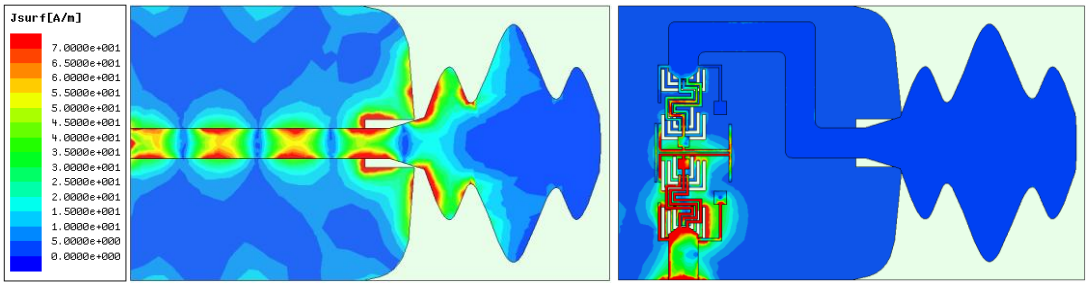

(a) (b)

Figure 5.18: Simulated surface current distributions of the proposed UWB antenna at a frequency of 18.5 GHz (an undesired response frequency without BPF) (a) Without UWB BPF, and (b) With UWB BPF.

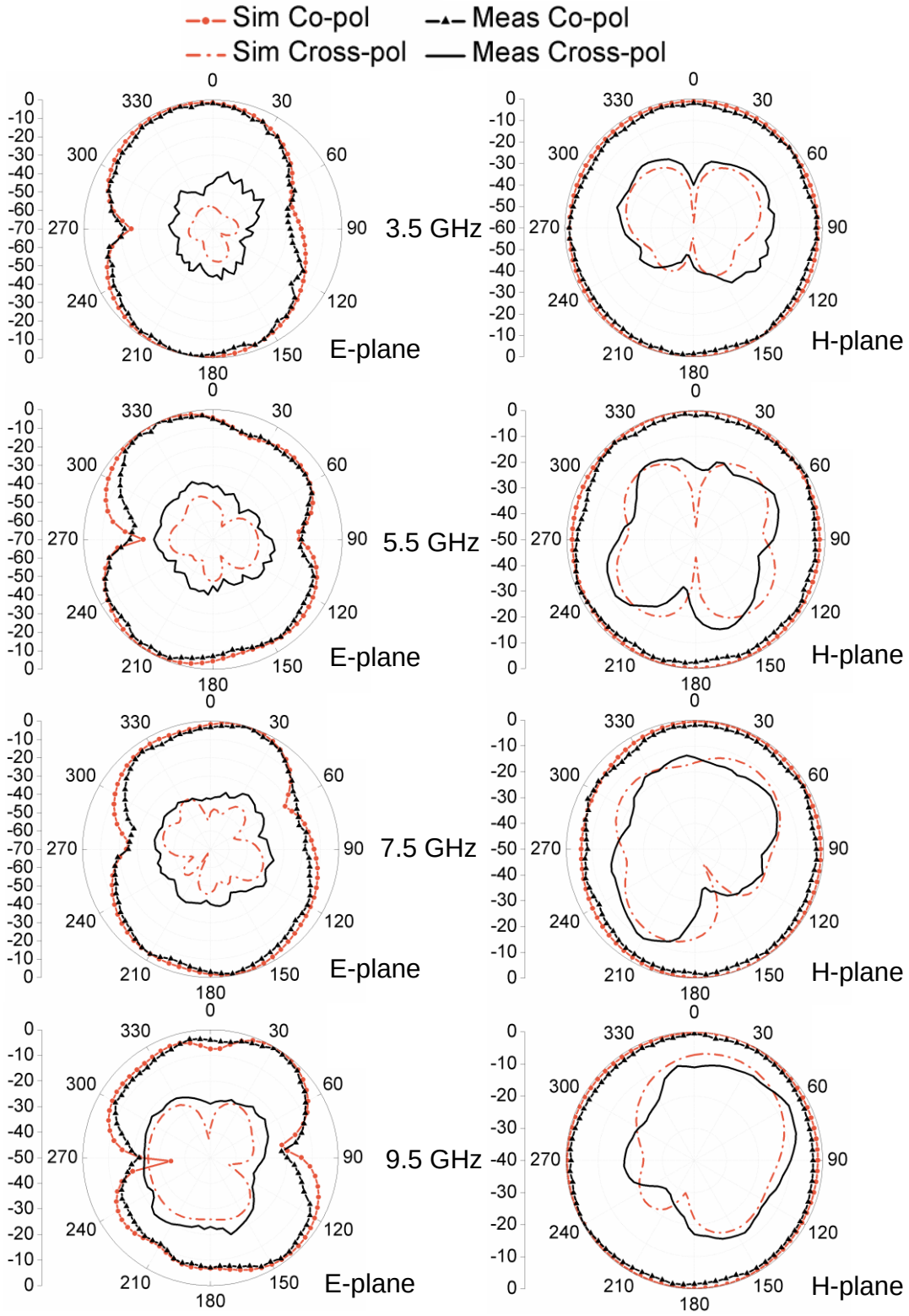

Figure 5.19: Numerically simulated and measured radiation patterns of the proposed UWB filtering antenna for four different frequencies.

5.4.2 Results and Discussion

5.4.2.1 Reflection Coefficient-Frequency Characteristics

Figure 5.16 shows the variations of reflection coefficient with frequency for the proposed UWB antenna with and without integration of the compact UWB BPF over the frequency band of interest. From Figure 5.16, it can be observed that the proposed UWB antenna with the UWB BPF (also called the proposed UWB filtering antenna) provides better selectivity at lower and upper edges of desired frequency band along with suppression of unwanted harmonics up to 30 GHz.

The numerically simulated and measured variations of the reflection coefficient of the proposed UWB filtering antenna with frequency are shown in Figure 5.17. Although the simulation study was carried out up to 30 GHz (as shown in Figure 5.16), experimental study was performed in the frequency range 2 – 18 GHz due to the limited operating frequency range of respective equipments/components available in our laboratory. The values of reflection coefficient of the proposed UWB filtering antenna were measured at different frequencies using Anritsu make VNA Master (Model: MS2038C). The simulated (measured) -10 dB reflection coefficient bandwidth of the proposed UWB filtering antenna covers the frequency range 3.07 – 10.72 GHz (3.08 – 10.69 GHz). It can be seen from Figure 5.17 that the simulated and measured results are nearly in agreement with each other over the frequency range of interest. The deviation in simulation and measured results is due to fabrication tolerances and measurement errors.

5.4.2.2 Simulated Surface Current Distributions

For better understanding of integration effectiveness of the proposed UWB BPF with the proposed UWB antenna for suppression of unwanted harmonics, the current

distributions on the surface of the proposed UWB antenna with and without the compact UWB BPF are studied. Figure 5.18 depicts the surface current distributions of the proposed UWB antenna with and without the UWB BPF at a frequency of 18.5 GHz (the frequency at and around which unwanted harmonics without BPF were observed through simulation). It can be noticed from Figure 5.18(a) that higher level of current reaches the modified elliptic-shaped radiating patch from input port in the absence of UWB BPF. Therefore, in order to suppress the harmonics, the UWB BPF is used to block the passage of current from the input port to radiating modified elliptic-shaped antenna. It can be clearly observed from Figure 5.18(b) that in presence of UWB BPF, the current is more concentrated near the BPF, and negligible current reaches the modified elliptic-shaped antenna at the frequency of 18.5 GHz (an undesired response frequency).

5.4.2.3 Radiation Patterns

The simulated and measured co- and cross-polarized radiation pattern plots of the proposed UWB filtering antenna in E- and H-planes for four different frequencies (3.5, 5.5, 7.5, 9.5 GHz) which are within operating frequency band are presented in Figure 5.19. From Figure 5.19, it can be observed that the proposed UWB filtering antenna has omni-directional co-polar radiation patterns with low cross-polarization levels at the frequencies considered in the study. The proposed UWB filtering antenna exhibits almost identical radiation patterns with tolerable cross-polarization levels when compared with the proposed UWB antenna without BPF presented in Figure 5.6 for same frequencies. It shows that the radiation characteristics of the proposed UWB filtering antenna are more or less maintained with good filtering characteristics over the UWB frequency band of interest.

5.4.2.4 Peak Realized Gain-Frequency Characteristics

Figure 5.20 shows the variations of simulated realized gain values of the proposed UWB antenna with and without integration of the compact UWB BPF with frequency. From Figure 5.20, it can be observed that the simulated gain values of the proposed UWB filtering antenna vary in the range 2.52 – 5.3 dB within its operating frequency band but drastic reduction in gain values occurs at lower and upper edges of the frequency band. Though the simulated realized gain values vary (in the range 2.26 – 5.2 dB) over the passband of isolated UWB antenna without UWB BPF similar to those for the proposed UWB filtering antenna, only little variation in its gain value occurs beyond the upper edge of desired frequency band (UWB). The proposed UWB filtering antenna provides simulated lowest and highest realized gain values of -8.9 dB and 0.9 dB at 11.7 GHz and 30 GHz respectively beyond the upper passband edge. In the case of the isolated UWB antenna without UWB BPF, simulated realized gain value at 11.7 GHz is 4.9 dB, which is 13.8 dB higher than that for the proposed filtering antenna. Further, the simulated lowest and highest realized gain values of the isolated UWB antenna beyond the upper passband edge are found to be 1.32 dB and 5.8 dB at 14.1 GHz and 30 GHz respectively.

The simulated realized gain value of -8.9 dB is obtained at 2.52 GHz below its lower passband edge of the proposed UWB filtering antenna. The simulated realized gain value for the isolated UWB antenna without UWB BPF at 2.52 GHz is 1.7 dB, which is 10.6 dB higher than that for the proposed UWB filtering antenna. This shows the performance superiority of the proposed filtering antenna over the isolated UWB antenna without BPF in terms of realized gain parameter.

Figure 5.21 shows the variations of simulated and measured realized gain values of the proposed UWB Filtering antenna with frequency. The simulated (measured)

realized gain values vary in the range 2.52 – 5.3 dB (2.51 – 5.2 dB) over the operating frequency band (3.07 – 10.72 GHz). The simulated and measured realized gain-frequency characteristics of the proposed UWB filtering antenna are nearly in agreement with each other.

5.4.2.5 Simulated Total Efficiency-Frequency Characteristic

Figure 5.22 shows the simulated variations of total efficiency of the proposed UWB antenna with and without integration of the UWB BPF with frequency. From Figure 5.22, it can be observed that the simulated total efficiency of the proposed integrated design of UWB filtering antenna vary in the range 84 – 91 % within its operating frequency band but drastic reduction in total efficiency occurs on either side of passband (= 3.07 – 10.72 GHz). The simulated total efficiency values vary in the range 89 – 94 % over the passband of isolated UWB antenna without BPF similar to those for the proposed UWB filtering antenna. It can be stated after comparing the total efficiency-frequency characteristics of the proposed UWB antenna with and without integration of the UWB BPF that significant suppression in the total efficiency value occurs above the desired passband in case of proposed UWB filtering antenna i.e. the proposed UWB antenna integrated with the proposed UWB BPF as compared with the isolated antenna without integration of UWB BPF. This shows the performance superiority of the proposed UWB filtering antenna over the isolated antenna without the proposed BPF in terms of total efficiency parameter. It is to be noted that total efficiency values in the UWB passband of the proposed filtering antenna are slightly less as compared with the isolated antenna due to somewhat better input impedance matching observed in case of isolated antenna [Figure 5.16].

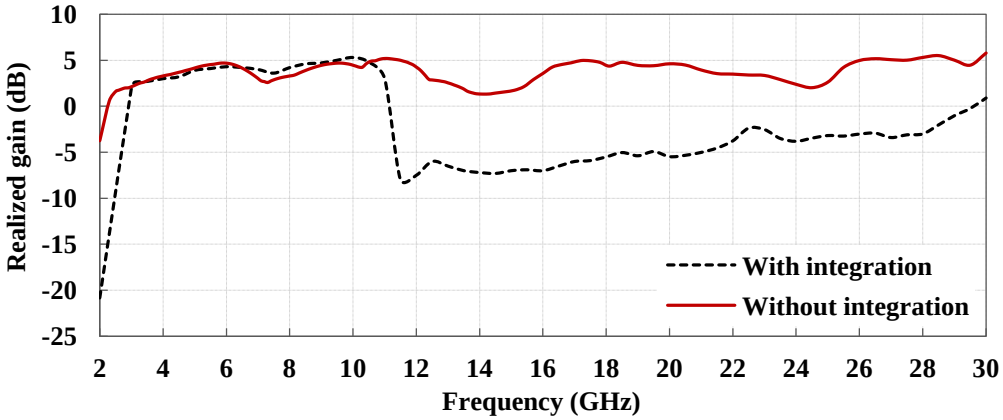

Figure 5.20: Numerically simulated gain values of the proposed UWB antenna with and without integration of the compact UWB BPF as a function of frequency.

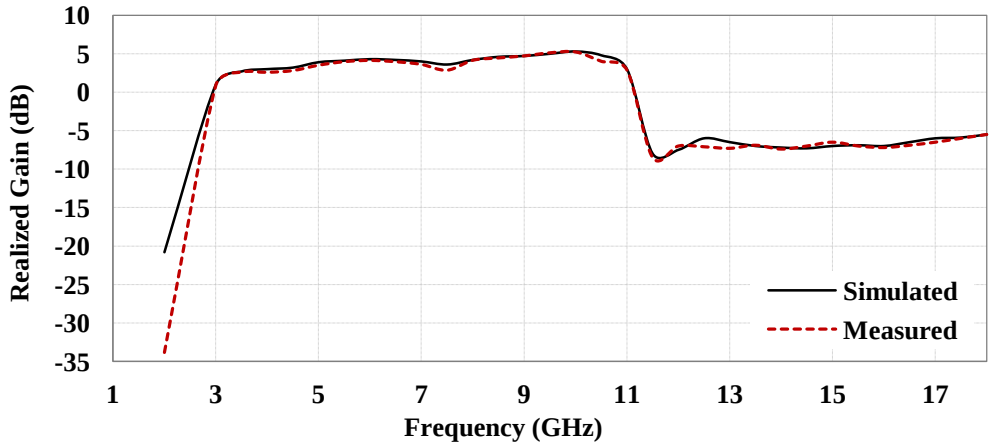

Figure 5.21: Numerically simulated and measured gain values of the proposed UWB filtering antenna as functions of frequency.

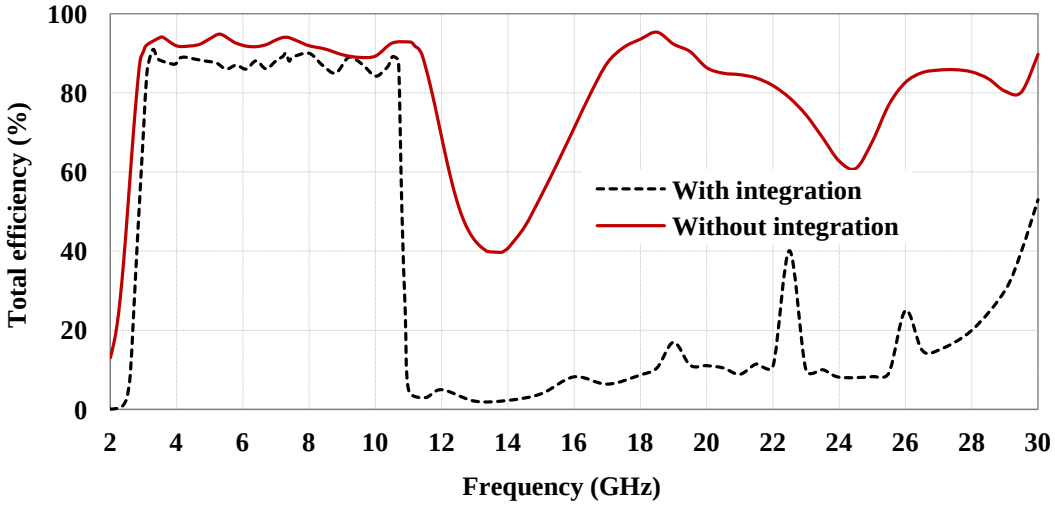

Figure 5.22: Numerically simulated variations of total efficiency of the proposed antenna with and without integration of the proposed UWB BPF versus frequency.

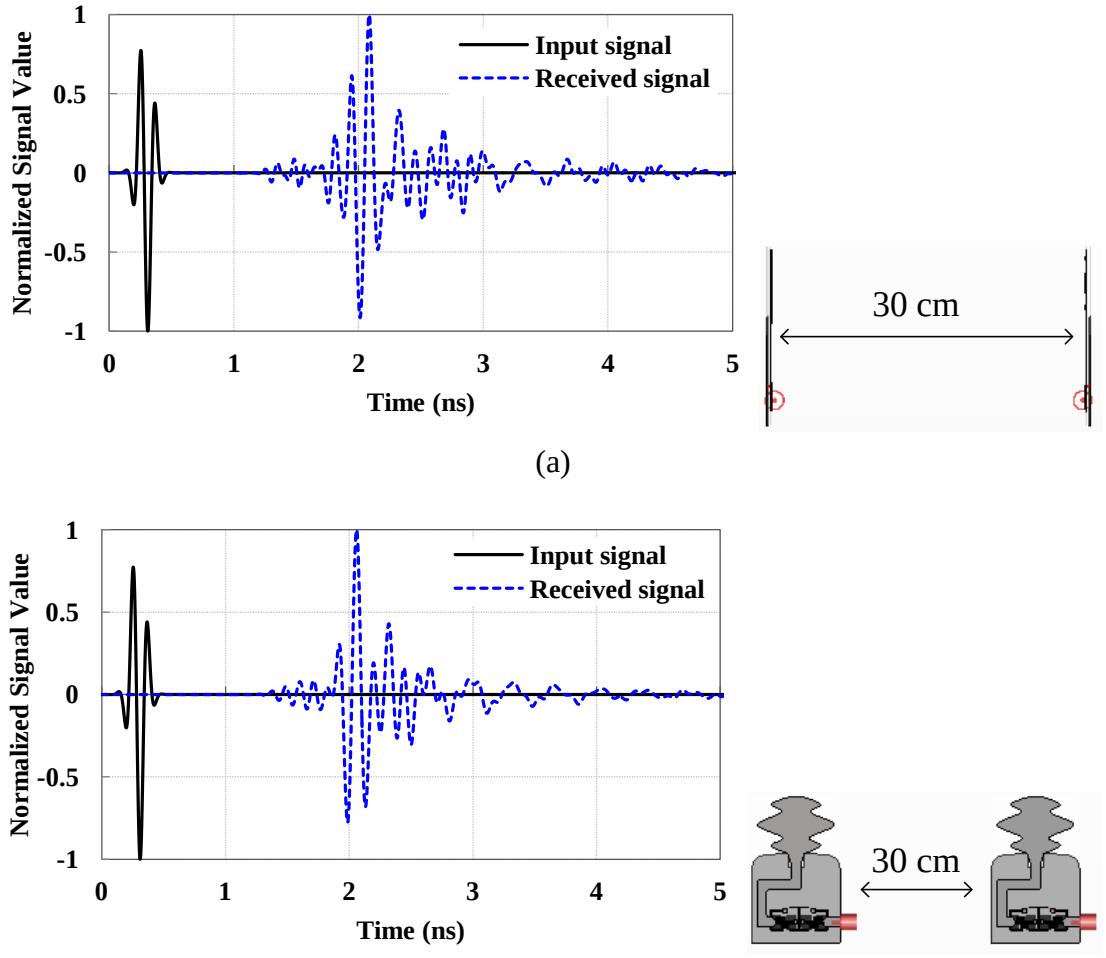

Figure 5.23: Excited and received pulses for different orientations of proposed UWB filtering antennas at a distance of 30 cm (a) face-to-face and (b) side-by-side.

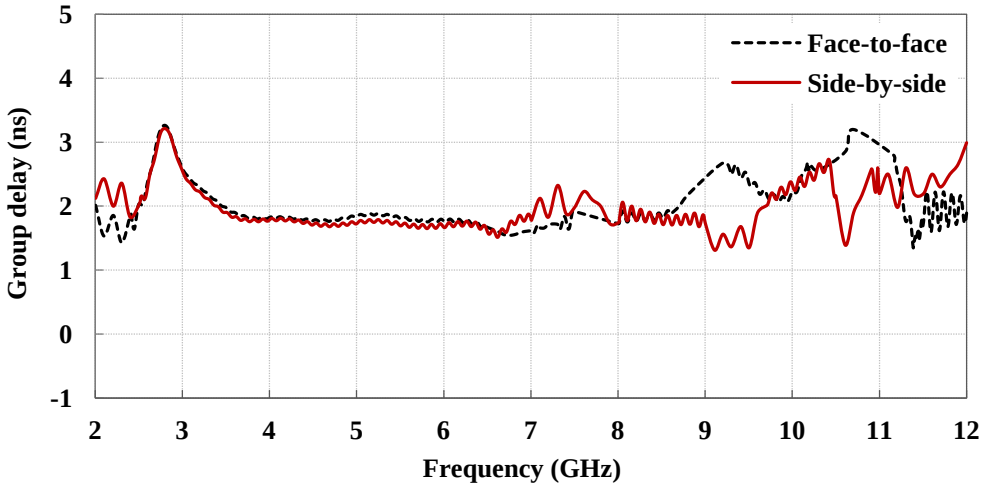

Figure 5.24: Simulated far-field group delays of the proposed UWB filtering antenna for different orientations at a distance of 30 cm.

5.4.2.6 Time Domain Analysis

It is imperative to study the pulse handling capability of the proposed UWB filtering antenna, as discussed for the proposed isolated UWB antenna in Section 5.2.2.4. It can be studied through time domain analysis and fidelity factor calculation in the far-field region in face-to-face and side-by-side orientations with respect to transmitting antenna using CST MWS software. The transmitting antenna was excited with Gaussian pulse and the signal was received at the receiving antenna kept at a distance of 30 cm in the far-field region. The normalized amplitudes of excited and received signals are shown in Figure 5.23. This figure depicts that the received pulse is somewhat stretched as compared with transmitted pulse, which indicates that received signal is somewhat distorted. In the case of isolated UWB antenna, received pulse is almost identical (as shown in Figure 5.9). This is because of better input impedance matching in case of isolated UWB antenna as compared with UWB filtering antenna.

The correlation between excited and received signals is calculated using SFF [Quintero et al. (2011)]. The SFFs in the case of face-to-face and side-by-side orientations of UWB filtering antennas are found to be 0.74 and 0.76 respectively. The calculated SFF values are near to 1, though less than those for isolated UWB antenna. This shows that the antenna has reasonable pulse handling characteristics.

Another important parameter of UWB filtering antennas is their almost constant group delay over the whole operating frequency band. The simulated values of far-field group delay of the proposed filtering antenna were obtained using arrangements of transmitting and receiving antennas identical to those employed for time domain analysis explained earlier. The simulated variations of far-field group delay of the proposed UWB filtering antenna for face-to-face and side-by-side configurations with frequency were determined through simulation using CST MWS software and the

results are provided in Figure 5.24. It can be seen from Figure 5.24 that the simulated values of far-field group delay of the proposed UWB filtering antenna vary in the range 1.3 − 3.3 ns for face-to-face and side-by-side configurations over the whole operating frequency band.

Table 5.6: Performance comparison of the proposed UWB filtering antenna with UWB filtering antennas reported in the literature.

Reference	**-10 dB impedance bandwidth (GHz)**	**Size (mm × mm)**	**Substrate dielectric constant, height (mm)**	**Harmonic suppression**
[Chen and Zhou (2009)]	3.3 – 10.4	44.2 × 31.2	4.5, 1.0	Upto 18 GHz
[Djaiz *et al*. (2011)]	3.1 – 10.6	68 × 27	2.2, 1.575	Upto 14 GHz
[Wong *et al*. (2013)]	3.1 – 10.6	28.5 × 28	2.55, 0.8	Upto 14 GHz
[Tang *et al*. (2016)]	2.995 – 11.047	37 × 25	3.48, 1.524	Upto 14 GHz
[Ranjan *et al*. (2017)]	3.31 – 11.01	32 × 27	3.38, 1.524	Upto 15 GHz
[Sahoo *et al*. (2017)]	3.1 – 10.6	53 × 42	2.55, 0.77	Upto 12 GHz
Proposed filtering antenna	**3.06 – 10.65**	**36 × 21**	**2.2, 0.787**	**Upto 30 GHz**

5.4.2.7 Performance Comparison of the Proposed UWB Filtering antenna with Those Reported in Literature

Finally, performance and dimension based comparison of the proposed UWB filtering antenna with those reported in the literature is given in Table 5.6. It is apparent from Table 5.6 that the proposed UWB filtering antenna is more compact and provides good harmonic suppression as compared with UWB filtering antennas reported in the literature.

5.5 Conclusion

A compact UWB filtering antenna having good cut-off performance and wide stopband with highly suppressed unwanted harmonics has been described in this chapter. The proposed UWB filtering antenna has been obtained through integration of the modified elliptic-shaped UWB antenna with the optimized version of compact UWB BPF reported in chapter 4. The modified elliptic-shaped patches and ground plane in the proposed UWB antenna are responsible for obtaining compact size antenna with good impedance matching over the desired UWB frequency band. Further, in order to get good selectivity and wide stopband with highly suppressed harmonics for the proposed UWB antenna, a compact UWB BPF has been integrated with it. The proposed UWB filtering antenna obtained through integration of the UWB antenna with the UWB BPF is compact in size with good band-edge selectivity and suppressed out-of-band harmonics up to 30 GHz. The proposed UWB filtering antenna and the UWB monopole antenna have been investigated through numerical simulation and/or measurements and the results have been found to be nearly in agreement with each other. It is finally concluded that the proposed compact UWB filtering antenna can be a good candidate for UWB systems.

Finally, chapter 6 summarizes and concludes the entire investigations presented in various chapters of the thesis. Chapter 6 also includes scope for further work, which is presented at the end of the chapter.